Photothermal electrostatics of the Pd-polyvinylidene fluoride photopyroelectric hydrogen gas sensor

Andreas Mandelis and Constantinos Christofides
Photoacoustic and Photothermal Sciences Laboratory, Department of Mechanical Engineering, and Center for Hydrogen and Electrochemical Studies (CHES), University of Toronto, Toronto, Ontario M5S 1A4, Canada

(Received 25 March 1991; accepted for publication 24 June 1991)

A detailed photothermal electrostatic consideration of the Pd-pyroelectric junction H_2 sensor is presented. Experimental evidence is in agreement with the fundamental features of the theory, which supports two possible mechanisms of ac-mode device operation: pyroelectric coefficient dependence on the hydrogenic dipole-induced charge density at the Pd-insulator polyvinylidene fluoride interface, and thermal-wave modulation of the hydrogen-concentration-dependent Pd work function. The dominant operating mechanism is found to depend on the experimental conditions. The concept of image dipole thermostatistical vibration and libration in the pyroelectric matrix is further successfully used to explain the temperature dependence of the photopyroelectric signal in support of the former above-mentioned mechanism.

I. INTRODUCTION

A recent development in photopyroelectric technology[1] has resulted in a sensitive solid-state device capable of monitoring minute concentrations of hydrogen gas under ambient pressure and temperature conditions.[2–4] The new sensor was found to be responsive down to 40 ppm of H_2 in N_2 at room temperature,[3] and the saturation photopyroelectric (PPE) signal exhibited Langmuirian behavior in the $\leqslant$200 Pa H_2 partial pressure range.[4] Those first reported results were hypothesized to be due to a mechanism, which involved a change in the pyroelectric coefficient of the polyvinylidene fluoride (PVDF) substrate of the sensor, proportional to the number density of the hydrogen atoms adsorbed and subsequently absorbed in the Pd ground electrode of the PVDF.

In this paper a detailed description of the photothermal electrostatics of the photopyroelectric junction device is given, which thus forms a rigorous basis for further investigations of the sensor mechanisms.

II. PHOTOTHERMAL ELECTROSTATICS OF THE METAL-PYROELECTRIC JUNCTION

The geometry of the Pd-PVDF H_2 sensor is shown in Fig. 1. This amounts to a capacitor consisting of Pd-electrode (ground; anode)/PVDF dielectric/Al-Ni-electrode (cathode). For a pyroelectric dielectric such as β-PVDF with a remanent frozen-in nonequilibrium polarization $\mathbf{P}$ due to an external electric field $\mathbf{E}_{\text{ext}}$, the Gibbs free energy is

$$G(T,\mathbf{E}_{\text{ext}}) = U - TS - \mathbf{P}\cdot\mathbf{E}_{\text{ext}}, \tag{1}$$

where U, T, and S are the total internal energy, the temperature, and the entropy of the pyroelectric. In Eq. (1) the piezoelectric properties of the pyroelectric have been ignored.[5] From the Second Law of Thermodynamics, the internal energy content change due to a change in polarization brought about by an external electric field is[6]

$$\Delta U = T\Delta S + \mathbf{E}_{\text{ext}}\cdot\Delta\mathbf{P}. \tag{2}$$

Equations (1) and (2) give for the concomitant variation in Gibbs' free energy:

$$\Delta G(T,\mathbf{E}_{\text{ext}}) = -S\Delta T - \mathbf{P}\cdot\Delta\mathbf{E}_{\text{ext}}. \tag{3}$$

Equation (3) helps define the polarization vector thermodynamically:

$$\mathbf{P} = \mathbf{P}(T,\mathbf{E}_{\text{ext}}) \equiv -\nabla_{\mathbf{E}} G(T,\mathbf{E}_{\text{ext}})|_T, \tag{4}$$

where

$$\nabla_{\mathbf{E}} \equiv \hat{i}\frac{\partial}{\partial E_x} + \hat{j}\frac{\partial}{\partial E_y} + \hat{k}\frac{\partial}{\partial E_z}. \tag{5}$$

Upon consideration of the polarization change, $\Delta\mathbf{P}$, in the pyroelectric element, due to variations in the temperature and electric field, T and $\mathbf{E}_{\text{ext}}$, one further obtains from a variation in Eq. (4)

$$\Delta\mathbf{P}(T,\mathbf{E}_{\text{ext}}) = \left(\frac{\partial\mathbf{P}}{\partial T}\bigg|_{\mathbf{E}_{\text{ext}}}\right)\Delta T + (\nabla_{\mathbf{E}}\cdot\mathbf{P}|_T):\Delta\mathbf{E}_{\text{ext}}. \tag{6}$$

Equation (6) is important in the present development in that it shows that under the most general thermodynamic equilibrium conditions, a change in the polarization vector of the pyroelectric is predicted if either the temperature or the external applied electric field, *or both*, are varied. The following definitions can now be made:

$$\mathbf{p}(T) \equiv \frac{\partial}{\partial T}\mathbf{P}(T,\mathbf{E}_{\text{ext}})|_{\mathbf{E}_{\text{ext}}} \tag{7}$$

for the pyroelectric coefficient vector of the material,[7] and

$$\boldsymbol{\epsilon}(\mathbf{E}_{\text{ext}}) \equiv \nabla_{\mathbf{E}}\cdot\mathbf{P}(T,\mathbf{E}_{\text{ext}})|_T \tag{8}$$

for the dielectric tensor:

$$\Delta\mathbf{P}(T,\mathbf{E}_{\text{ext}}) = \mathbf{p}(T)\Delta T + \boldsymbol{\epsilon}(\mathbf{E}_{\text{ext}}):\Delta\mathbf{E}_{\text{ext}}. \tag{9}$$

 0021-8979/91/084496-09$03.00

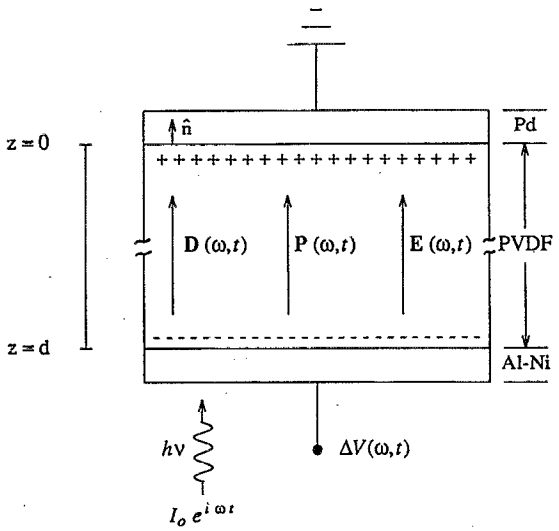

FIG. 1. PPE H_2 capacitive sensor. The Pd anode (ground electrode) is in contact with the Inficon™ housing of the sensor. The cathode (back electrode) is the standard Pennwalt Al-Ni layered electrode (see Ref. 2). Intermittent photothermal excitation of intensity I_0 at frequency $f=\omega/2\pi$ is assumed from the rear side of the capacitor.

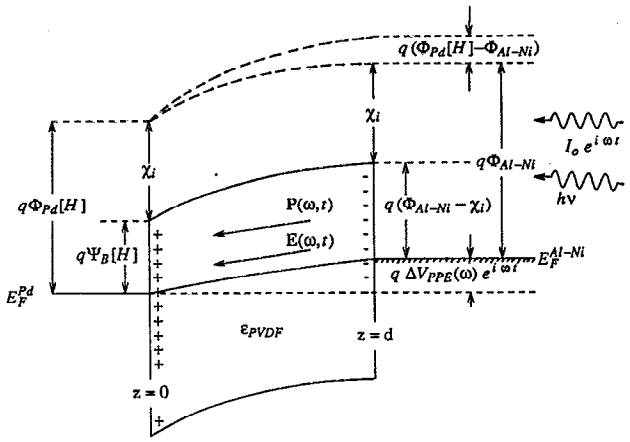

FIG. 2. Energy-band structure of the PPE H_2 sensor device. E_F^j: Fermi level of metal $j[j=$ Pd, Al-Ni; χ_i: electron affinity of the insulator (PVDF film)]; $\phi_{Pd}[H]$: Pd work function, a function of hydrogen concentration in the catalytic metal; $\Psi_B[H]$: potential barrier height between the Pd Fermi level and the conduction band of the insulator; $\phi_{Al\text{-}Ni}$: work function of the layered electrode of the anode. The curvature of the bands is parabolic. Intermittent photothermal excitation is assumed from the Al-Ni electrode side.

In the absence of an applied external field, i.e., for $\Delta\mathbf{E}_{ext}=\mathbf{0}$, a photothermal modulation of the structure in Fig. 1 results in synchronous oscillation of the generally depth-dependent polarization vector. From Eq. (9),

$$\Delta\mathbf{P}(\omega,z,t)=\mathbf{p}(T,z)\Delta T(\omega,z,t). \tag{10}$$

This amounts to a depth-dependent oscillating internal electric field given by[6]

$$\Delta\mathbf{E}(\omega,z,t)=(1/\epsilon_0)\chi_e^{-1}:\mathbf{p}(T,z)\Delta T(\omega,z,t), \tag{11}$$

with χ_e the electric susceptibility tensor. To facilitate further analysis, without loss of the general physics of the situation, the photothermally excited pyroelectric will be subsequently assumed to behave *linearly* and *isotropically* for low incident optical irradiances I_0 (Fig. 1). Under these conditions both ϵ and χ_e tensors are reduced to scalars, and the potential difference $\Delta V(\omega,t)$ developed across the pyroelectric capacitor photothermally is

$$\Delta V(\omega,t)=-\int_d^0 \Delta\mathbf{E}(\omega,z,t)\cdot d\mathbf{r}\simeq\frac{p_z}{\chi_e\epsilon_0}\int_0^d \Delta T(\omega,z,t)\,dz, \tag{12}$$

where the component of the pyroelectric coefficient vector along the line of integration (z axis) is given as

$$\mathbf{p}\cdot d\mathbf{r}=p_z\,dz \tag{13}$$

and is assumed to be independent of the coordinate for linear, isotropic, and homogeneous pyroelectrics. In the geometry of Fig. 1, and assuming deposition of the irradiance-modulated optical energy on the opaque, blackened thin-film Al-Ni electrode, the thickness of which ($\sim$a few hundred Ångstroms) is negligible compared to that of the PVDF, the photothermal-wave field in the pyroelectric is found to be [8]

$$\Delta T(\omega,z,t)=\Delta T_0(\omega)e^{-(1+i)a_p(\omega)(d-z)+i\omega t}. \tag{14}$$

Equations (12)–(14) now give the average ac potential difference generated photopyroelectrically across the capacitor:

$$\Delta V(\omega,t)=\Delta V_{PPE}(\omega)e^{i\omega t}, \tag{15a}$$

where

$$\Delta V_{PPE}(\omega)=-I_0\frac{i\eta p_z(1-e^{-(1+i)a_p(\omega)d})}{4\chi_e\epsilon_0 k_p(1+g)\alpha_p^2(\omega)} \tag{15b}$$

is the complex amplitude of the PPE potential; η is the nonradiative (optical-to-thermal) energy conversion efficiency; k_p is the thermal conductivity of the pyroelectric; g is a backing-to-pyroelectric thermal coupling coefficient;[8] and $a_p(\omega)$ is the thermal diffusion coefficient in the PVDF given by

$$a_p(\omega)=(\omega/2\alpha_p)^{1/2}, \tag{16}$$

and α_p is the thermal diffusivity of the pyroelectric.

The ac photothermal potential oscillation of Eq. (15) modulates the energy-band diagram of Fig. 1, which consists of a catalytic metal-insulator-inert metal structure, as shown in Fig. 2. In constructing the band structure of the H_2 sensor, the following were taken into account: (a) The well-known[9] decrease of the Pd work function, $q\phi_{Pd}$, in the presence of a hydrogen concentration in the Pd matrix, which forms a dipole layer at the Pd-insulator interface, as

observed conclusively with the Pd-SiO_2 interface.[10–12] The work-function decrease can be written

$$q\phi_{\mathrm{Pd}}[\mathrm{H}]=q(\phi_{\mathrm{Pd}}[0]-\Delta V[\mathrm{H}]); \tag{17}$$

(b) the photothermal potential modulation of the energy levels of the pyroelectric due to the incident optical irradiance $I_0e^{i\omega t}$, which results in an effective potential source given by Eq. (15); and (c) the existing contact potential difference between the anode (Pd) and cathode (Al-Ni) metals:

$$q\phi_0[\mathrm{H}]=q(\phi_{\mathrm{Pd}}[\mathrm{H}]-\phi_{\mathrm{Al\text{-}Ni}})=q(\phi_0[0]-\Delta V[\mathrm{H}]). \tag{18}$$

The electrostatic potential function across the device structure, which determines the curvature of the energy-band diagram in Fig. 2, can be calculated as a linear superposition of the three effects outlined above. Assuming potential invariance along the lateral (x,y) dimensions, consistent with the thin-film nature of the pyroelectric PVDF, the various contributions to the potential field are as follows.

A. Contact potential

In both conducting electrodes, Pd and Al-Ni, the absence of internal electric fields, when not exposed to H_2 atmosphere, can be expressed as boundary conditions to the electrostatic contact potential $\phi_0(z)$:

$$\frac{d}{dz}\phi_0(z)|_{z=0}=\frac{d}{dz}\phi_0(z)|_{z=d}=0 \tag{19}$$

or

$$\phi_0(0)=\mathrm{const}=\phi_{\mathrm{Pd}}[0],\quad \phi_0(d)=\mathrm{const}=\phi_{\mathrm{Al\text{-}Ni}}. \tag{20}$$

In the region $0<z<d$ no free charges exist, and thus the displacement vector satisfies

$$\frac{\partial}{\partial z}(\hat{n}\cdot\mathbf{D})=-\frac{\partial}{\partial z}(\epsilon\hat{n}\cdot\nabla\phi_0)=0. \tag{21}$$

Since a homogeneous pyroelectric was assumed,

$$\frac{\partial\epsilon}{\partial z}=0, \tag{22}$$

so that

$$\frac{\partial^2}{\partial z^2}\phi_0(z)=0, \tag{23}$$

subject to Eq. (20). The solution is

$$\phi_0(z)=\phi_{\mathrm{Pd}}[0]+\Delta\phi_0(z/d), \tag{24}$$

where

$$\Delta\phi_0[0]\equiv\phi_{\mathrm{Al\text{-}Ni}}-\phi_{\mathrm{Pd}}[0] \tag{25}$$

is the contact potential difference between the two electrodes in the absence of H_2 and is expected to be negative, as $\phi_{\mathrm{Pd}}>\phi_{\mathrm{Al}}$ when measured in vacuum and for clean metal surfaces.[13]

B. Photopyroelectric potential

Physically, the thermal-wave field in the pyroelectric results in synchronous, albeit out of phase, expansions and contractions of both electrode-pyroelectric junction interface areas during one heating and cooling cycle. For very thin PVDF films under thermally thin conditions,[8] these mechanical motions occur approximately simultaneously on both sides of the film and result in excess free-surface charge densities at both positive and negative junctions of Fig. 1. The free-charge densities on the metal-side, in turn, induce bound excess surface densities, $\sigma_{\mathrm{PPE}}(\omega,t)$, on the insulator side of the junction, such that

$$\sigma_{\mathrm{PPE}}^{(+)}=|\sigma_{\mathrm{PPE}}^{(-)}|\equiv\sigma_{\mathrm{PPE}}(\omega,t). \tag{26}$$

These PPE-induced charge densities change the boundary conditions for the polarization vector in the bulk of the pyroelectric through what amounts to a modulation of the total charge density in the capacitor plates. Otherwise, no change in the bound charge density in the bulk occurs, as the charge modulations at both interfaces are symmetric and their effects cancel each other out. The polarization satisfies

$$\frac{\partial}{\partial z}(\hat{n}\cdot\mathbf{P}_{\mathrm{PPE}})=-\frac{\partial}{\partial z}(\epsilon_0\chi_e\hat{n}\cdot\nabla\phi_{\mathrm{PPE}})=0, \tag{27a}$$

where the constitutive equation for the polarization vector in a linear isotropic pyroelectric

$$\mathbf{P}=-\chi_e\epsilon_0\nabla\phi \tag{27b}$$

was used. Due to the assumed homogeneity,

$$\frac{\partial\chi_e}{\partial z}=0, \tag{28}$$

so that

$$\frac{\partial^2}{\partial z^2}\phi_{\mathrm{PPE}}(z)=0. \tag{29}$$

Furthermore, the application of Gaussian pillboxes across the interfaces at $z=0$ and $z=d$, along with $\mathbf{P}=\mathbf{0}$ in the conducting electrodes of Fig. 1, yields

$$\hat{n}\cdot\mathbf{P}_{\mathrm{PPE}}=P_n^{(\mathrm{PPE})}(0)=\sigma_{\mathrm{PPE}}^{(+)}(\omega,t),\quad z=0, \tag{30a}$$

$$\hat{n}\cdot\mathbf{P}_{\mathrm{PPE}}=P_n^{(\mathrm{PPE})}(d)=\sigma_{\mathrm{PPE}}^{(-)}(\omega,t),\quad z=d, \tag{30b}$$

Now the complete solution of Eq. (29), subject to the boundary conditions (30) via Eq. (27b), is

$$\phi_{\mathrm{PPE}}(z;\omega,t)=-\frac{\sigma_{\mathrm{PPE}}(\omega,t)}{\epsilon_0\chi_e}z. \tag{31}$$

The bound charge density on the high-resistivity insulating pyroelectric side of the interface is related to the free-surface charge density via[6]

$$\sigma_{\mathrm{PPE}}(\omega,t)=-\left(\frac{\chi_e\epsilon_0}{\epsilon}\right)\sigma_f^{(\mathrm{PPE})}(\omega,t), \tag{32}$$

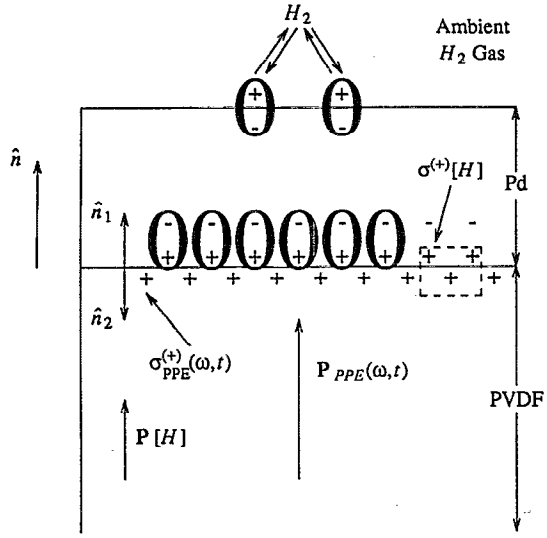

FIG. 3. Schematic of the formation of bound hydrogen dipoles at the Pd-PVDF interface $z=0$, and Gaussian pillbox for the calculation of the polarization.

so that the measurable net potential difference across the device due to the photopyroelectric effect is

$$\Delta V(\omega,t)=\phi_{\mathrm{PPE}}(d;\omega,t)-\phi_{\mathrm{PPE}}(0;\omega,t)=\frac{\sigma_f^{(\mathrm{PPE})}(\omega,t)d}{\epsilon}. \tag{33}$$

A comparison of Eqs. (15), (32), and (33) shows that the photopyroelectrically induced average complex surface charge density at the two junctions ($z=0$ and $z=d$) has amplitude and phase given by

$$\sigma_f^{(\mathrm{PPE})}(\omega,t)=-I_0 i\eta p_z\left(\frac{1-e^{-(1+i)a_p(\omega)d}}{4k_p d(1+g)a_p^2(\omega)}\right)e^{i\omega t}. \tag{34}$$

C. Hydrogen-induced potential

For the Pd-PVDF junction with the positive bound charge density of the poled β-PVDF facing the junction, as in Fig. 1, adsorbed and absorbed H atoms are assumed to give rise to a dipole field in the Pd electrode due to a displacement of the electronic cloud surrounding the nucleus[14] away from the junction and into the metal (s adsorption). This configuration is schematically shown in Fig. 3 and is consistent with experimental evidence at the Pd-SiO_2 insulator junction, in the metal-oxide-semiconductor (MOS) H_2-sensor field,[15] as well as with earlier results with the PPE-PVDF sensor.[2] With the aid of the Gaussian pillbox in Fig. 3, the value of the polarization at the Pd-PVDF junction can be written

$$\hat{n}\cdot\mathbf{P}[\mathrm{H}]=P_{n0}[\mathrm{H}]=\sigma^{(+)}[\mathrm{H}],\quad z=0. \tag{35}$$

The hydrogen-absorption-related charge density $\sigma^{(+)}[\mathrm{H}]$ at this junction will be unbalanced with respect to the opposite electrode at $z=d$; therefore, it will generate (induce) a bulk polarization gradient, which results in a new distribution of bound volume charge densities, $\rho_b[\mathrm{H}]$:

$$\frac{\partial}{\partial z}(\hat{n}\cdot\mathbf{P}[\mathrm{H}])=\frac{\partial}{\partial z}P_{n0}(z;[\mathrm{H}])=-\rho_b[\mathrm{H}]. \tag{36}$$

Equation (36) is subject to the condition $P_{n0}(d;[\mathrm{H}])=0$, since the back interface is unaffected by the presence of hydrogen. Now Eqs. (27b), (28), and (36) yield

$$\frac{\partial^2}{\partial z^2}\phi_{[\mathrm{H}]}(z)=\frac{1}{\epsilon_0\chi_e}\rho_b[\mathrm{H}], \tag{37}$$

with the solution

$$\phi_{[\mathrm{H}]}(z)=-\frac{\sigma^{(+)}[\mathrm{H}]z}{\chi_e\epsilon_0}+\frac{\sigma^{(+)}[\mathrm{H}]z^2}{2\chi_e\epsilon_0 d}, \tag{38}$$

where, from Eqs. (35) and (36),

$$\rho_b[\mathrm{H}]=\frac{\sigma^{(+)}[\mathrm{H}]}{d} \tag{39}$$

and the junction at $z=0$ was assumed grounded, i.e., $\phi_{[\mathrm{H}]}(0)=0$. It is the dependence of $\phi_{[\mathrm{H}]}$ on z described by Eq. (38) on which the parabolic structure of the energy bands in Fig. 2 is based, superposed on the linearity predicted by Eqs. (24) and (31). The potential difference across the device due to the induced bound charge by the hydrogen dipole layer is

$$\Delta V_b[\mathrm{H}]=-\frac{\sigma^{(+)}[\mathrm{H}]d}{2\chi_e\epsilon_0}, \tag{40}$$

or, in keeping with the (induced bound insulator charge)↔(free-electrode charge) analogy of Eq. (32), the measurable potential difference is

$$\Delta V[\mathrm{H}]=\frac{\sigma_f^{(+)}[\mathrm{H}]d}{2\epsilon}. \tag{41}$$

Finally, linear superposition of all the relevant potential fields, Eqs. (24), (33), and (41), gives

$$\Delta V(\omega,[\mathrm{H}];t)=(d/\epsilon)\sigma_f^{(\mathrm{PPE})}(\omega,t)+(d/2\epsilon)\sigma_f^{(+)}[\mathrm{H}]+\Delta\phi_0[\mathrm{H}], \tag{42}$$

where in Eq. (25) allowance was made for the possibility that the Pd work function may depend on the absorbed hydrogen concentration:[9]

$$\Delta\phi_0[\mathrm{H}]=\phi_{\mathrm{Al\text{-}Ni}}-\phi_{\mathrm{Pd}}[\mathrm{H}]. \tag{25'}$$

In synchronous lock-in operation of the device, the middle term on the right-hand side (rhs) of Eq. (42) must be omitted as it represents a dc potential contribution. Therefore, the observed dependence of the PPE signal on the hydrogen concentration must involve either the first term (which should carry an [H] dependence), or the third term (which should carry an ω dependence) or both.

1. [H] dependence of $\sigma_f^{(PPE)}(\omega,t)$

It was shown above that the presence of an unbalanced dipole layer in the vicinity of the Pd-PVDF interface produces a net change $\mathbf{P}[\mathrm{H}]$ in the original oscillating polarization of the pyroelectric setup by the PPE effect

$$\mathbf{P}(\mathbf{r}) = \mathbf{P}_{\mathrm{PPE}}(\omega,t) + \mathbf{P}(\mathbf{r};[\mathrm{H}]), \tag{43}$$

as shown in Fig. 3. Equations (36) and (39) give the magnitude of this excess polarization:

$$\hat{n}\cdot\mathbf{P}(\mathbf{r};[\mathrm{H}]) = P_{n0}(z;[\mathrm{H}]) = [1-(z/d)]\sigma^{(+)}[\mathrm{H}]. \tag{44}$$

The net average polarization change in the pyroelectric is given by

$$\langle P_{n0}[\mathrm{H}]\rangle = \frac{1}{d}\int_0^d P_{n0}(z;[\mathrm{H}])\,dz = \tfrac{1}{2}\sigma^{(+)}[\mathrm{H}]. \tag{45}$$

This result combined with Eq. (30) can be used to describe the total polarization field, Eq. (43):

$$\langle P_n\rangle = \tfrac{1}{2}\sigma^{(+)}[\mathrm{H}] + P_n^{(\mathrm{PPE})}, \tag{46}$$

where the definition of Eq. (26) was used to denote either Eq. (30a) or (30b) through the $P_n^{(\mathrm{PPE})}$ term. In terms of hydrogenic electric dipoles, the portion of the polarization vector contributed by the hydrogen presence at the junction can be written[16]

$$\mathbf{P}(\mathbf{r};[\mathrm{H}]) = \sum_i n_i[\mathrm{H}]\langle\mathbf{m}_i(\mathbf{r})\rangle, \tag{47}$$

where $n_i[\mathrm{H}]$ is the population of hydrogen dipoles in state (i) and $\langle\mathbf{m}_i(\mathbf{r})\rangle$ is the average of the hydrogenic dipole moment in state (i), a function of its position $\mathbf{r}$. Upon taking the thermal average of $\hat{n}\cdot\mathbf{P}(\mathbf{r};[\mathrm{H}])$ at thermodynamic equilibrium temperature T, one obtains

$$\begin{aligned}\langle P_n[\mathrm{H}]\rangle_T &= \hat{n}\cdot\Big\langle\sum_i n_i[\mathrm{H}]\langle\mathbf{m}_i(\mathbf{r})\rangle\Big\rangle_T \\ &\simeq \hat{n}\cdot\langle\langle\mathbf{m}_i(\mathbf{r})\rangle\rangle_T\Big(\sum_i n_i[\mathrm{H}]\Big) \\ &= \langle m_z\rangle_T N_{\mathrm{H}},\end{aligned} \tag{48}$$

where

$$N_{\mathrm{H}} = \sum_i n_i[\mathrm{H}]$$

is the total number density of hydrogenic dipoles thermally averaged over all thermodynamic microstates, and $\langle m_z\rangle_T$ is the average component of the dipole moment along the z axis at temperature T. Finally, it can be recognized that the thermal average of the microscopic polarization, Eq. (48), is the same as the macroscopic phenomenological quantity of Eq. (45), and one may thus write for the average interfacial charge density due to the dipoles:

$$\sigma^{(+)}[\mathrm{H}] = 2N_{\mathrm{H}}\langle m_z\rangle_T. \tag{49}$$

The thermalization of the microscopic hydrogenic dipole moment $\langle\mathbf{m}\rangle_T$ precisely defines the thermodynamic temperature dependence of the polarization. Using the thermodynamic definition of the pyroelectric coefficient vector, Eqs. (7) and (46), it is easy to show that

$$\begin{aligned}p_z[\mathrm{H}] = \hat{n}\cdot\mathbf{p}(T) &= \frac{\partial}{\partial T}(N_{\mathrm{H}}\langle m_z\rangle_T) + \frac{\partial}{\partial T}P_n^{(\mathrm{PPE})} \\ &= N_{\mathrm{H}}\left(\frac{\partial}{\partial T}\langle m_z\rangle_T - \alpha_v\langle m_z\rangle_T\right) + p_z[0].\end{aligned} \tag{50}$$

In Eq. (50) α_v is the relative thermal expansion coefficient of PVDF,

$$\alpha_v = V^{-1}(\partial V/\partial T) \tag{51}$$

and $p_z[0]$ is the value of the z component of the pyroelectric coefficient vector in the absence of hydrogenic dipoles. It is also assumed that the temperature oscillation due to the thermal wave does not measurably affect the value of $\mathbf{p}(T)$. Equation (50) demonstrates that an [H] dependence of $\sigma_f^{(\mathrm{PPE})}(\omega,t)$ in Eq. (34) is possible through the dependence of the pyroelectric coefficient on the number density N_{H} of hydrogen dipoles at the Pd-PVDF junction interface. Furthermore, Eq. (50) helps give physical meaning to the quantity $(\partial p_z/\partial N_{\mathrm{H}})$ used in earlier work[2,4] in order to postulate the pyroelectric coefficient dependence on N_{H}, as

$$\left.\frac{\partial p_z}{\partial N_{\mathrm{H}}}\right|_{N_{\mathrm{H}}=0} = \frac{\partial}{\partial T}\langle m_z\rangle_T - \alpha_v\langle m_z\rangle_T. \tag{52}$$

An important consequence of this model is that in the limit of a photothermal modulation frequency range in which the pyroelectric is thermally thick,[8] it predicts an output voltage amplitude modulation frequency dependence

$$|\Delta V_I(\omega,[\mathrm{H}])| = \frac{I_0\eta\alpha_p}{\epsilon(1+g)k_p\omega}p_z[\mathrm{H}] \propto \omega^{-1}, \tag{53}$$

as shown from Eq. (34) with $a_p(\omega)d \gg 1$, and the first rhs term of Eq. (42).

2. ω dependence of $\Delta\phi_0(H)$

The frequency dependence of the contact potential difference between catalytic Pd and inert metal Al-Ni electrode can be obtained upon consideration of the temperature dependence of the Pd work function:

$$q\phi_{\mathrm{Pd}}[\mathrm{H}] = q\phi_{\mathrm{Pd}}([\mathrm{H}],T). \tag{54}$$

With small-amplitude temperature modulation of the junction at $z=0$, it can be seen that Eq. (25′) becomes

$$\delta(\Delta\phi_0\{[\mathrm{H}],T(\omega)\}) = -\frac{\partial}{\partial T}\phi_{\mathrm{Pd}}([\mathrm{H}],T)|_{T=T_0}\Delta T(\omega), \tag{55}$$

and $\Delta T(\omega)$ is given by Eq. (14) evaluated at $z=0$. The thermal-wave modulation of the contact potential difference will then produce an ac contribution to the third term on the rhs of Eq. (42) with voltage amplitude

$$|\Delta V_{\rm III}(\omega,[{\rm H}])| = -\left(\frac{\partial}{\partial T}\phi_{\rm Pd}([H],T)|_{T=T_0}\right)\Delta T_0(\omega) \times \exp\left[-\left(\frac{\omega}{2\alpha_p}\right)^{1/2} d\right], \quad (56a)$$

with

$$\Delta T_0(\omega) \simeq \frac{-I_0\eta}{2(1+g)k_p a_p^2(\omega)} \quad (56b)$$

for a thermally thick pyroelectric. A similar mechanism was proposed qualitatively in order to explain the sensitivity to ambient H_2 of a Pd-mica-inert electrode (gold) capacitor.[17] In that device there can be no PPE effect, and thus this can be the only source of a synchronous voltage dependence on [H] through the temperature derivative in the large parentheses of Eq. (56a). It is important to note that the modulation frequency dependence of $|\Delta V_{\rm III}|$ is $\sim\omega^{-1}\times\exp(-K\sqrt{\omega})$ in this model, as the thermomodulation of the Pd work function is only affected by the tail of the exponentially damped thermal-wave distribution within the bulk of the dielectric. Therefore, in principle, the frequency dependence of the PPE device signal, where both mechanisms expressed by Eqs. (53) and (56) are possible, can resolve which one is dominating the operation of the Pd-PPE sensor.

III. EXPERIMENT AND DISCUSSION

The experimental system and sensor particulars have been described in detail elsewhere.[2-4] Polyvinylidene fluoride (PVDF) thin film of 28 μm thickness was used as the pyroelectric insulator forming a junction with 130-Å-thick Pd. 100% H_2 gas was introduced in the chamber and the PPE signal from an IR semiconductor laser diode source was monitored as a function of frequency or temperature. All experiments were performed after cleansing with a N_2 gas stream all ambient gases, as well as the Pd surface. No reference detector was used for these experiments at 100% H_2. The frequency-dependent measurements were carried out under two distinctly different conditions. One set of experiments involved introducing H_2 gas at a low modulation frequency and, upon reaching the saturation response level,[4] the frequency was increased under continuous H_2 flow to the limit where no measurable difference could be observed between the hydrogen-saturated device and a background signal obtained in the presence of N_2 gas only. The results are shown plotted in Fig. 4(a) versus f^{-1}. It was observed that the PPE voltage obeyed approximately the frequency dependence of the substrate (pyroelectric) as shown in Fig. 4(b) in the thermally thick regime, i.e., for

$$f \gg f_c \equiv \alpha_p/\pi d^2 \simeq 22 \text{ Hz}. \quad (57)$$

A PPE signal due to H_2 absorption could be measured up to 380 Hz. The ratio of PPE voltage in the presence of H_2 to the voltage in ambient N_2 in Fig. 4(b) normalizes out the instrumental and geometric frequency dependences of the sensor-detection system. The slopes of both voltages in Fig. 4(a) in the thermally thick regime were somewhat

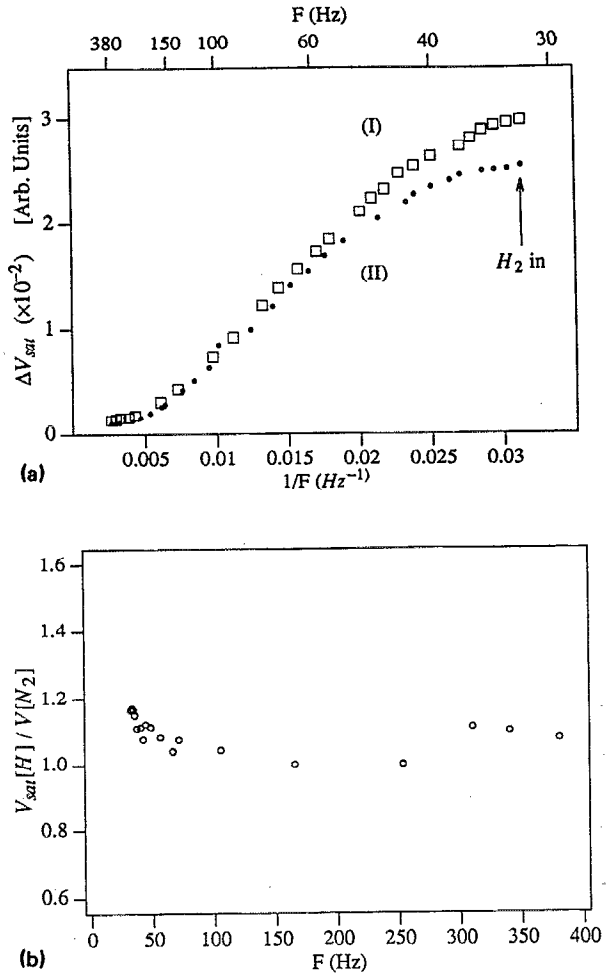

FIG. 4. (a) PPE saturation signal vs frequency: (I) 100% H_2 was introduced at $f = 32$ Hz and frequency was increased under constant H_2 flow of 500 ml/min; (II) reference curve in 100% N_2. (b) Ratio of the two signals of (a).

different from the predicted ω^{-1} dependence of Eq. (53), and the discrepancy was traced back to the violation of the one-dimensional assumption under which Eq. (53) was derived: In our experiments the optical fiber source size was on the order of one thermal diffusion length (a_p^{-1}), which rendered the problem three-dimensional, with an effect on the exponent of the algebraic frequency dependence of the signal. Overall, the important message of Fig. 4 is that the hydrogenic PPE voltage behaves consistently with a bulk pyroelectric effect, with an [H] dependence due to the change in the pyroelectric coefficient value.

A separate set of experiments involved measuring the H_2 saturation voltage at each modulation frequency, then removing the hydrogen gas from the chamber, changing the frequency, and repeating the measurement. The results are shown in Fig. 5, which suggests an exponential decay of the saturation PPE signal with $f^{1/2}$ in the thermally thick regime. It is interesting to note that in this experimental mode the rapid decay of the differential PPE signals with increasing frequency is qualitatively, at least in agreement with a similar observation reported at 5% H_2 in N_2 with the Pd-mica-Au sensor.[17] The slopes of the two curves

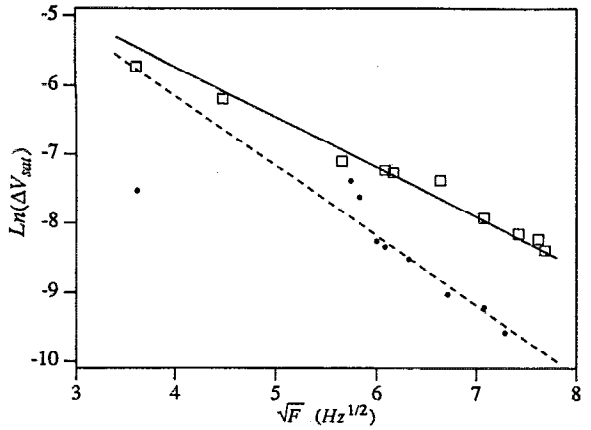

FIG. 5. PPE saturation signal vs frequency: 100% H_2 was introduced at each frequency at 500 ml/min, and was cycled out of the system before each frequency change. Upper curve: 28-μm-thick PVDF, 1588-Å-thick Pd; lower curve: 52-μm-thick PVDF, 130-Å-thick Pd.

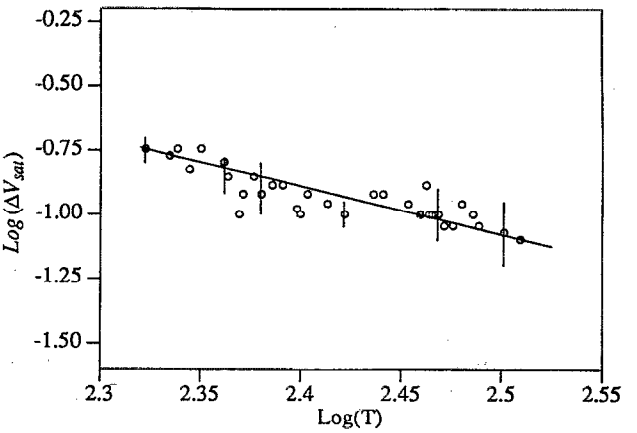

FIG. 6. Temperature dependence of H_2 saturation PPE voltage, ΔV_{sat}, at 32 Hz. The curve was obtained after subtracting the background signal upon evacuation of the H_2 from the chamber and replacement with N_2 gas.

in Fig. 5 were found to give, according to Eq.(56a), thermal diffusivities for PVDF approximately a factor of 3 (52-μm film) and 10 (28-μm film), respectively, lower than the accepted value of[8] 5.4×10^{-8} m^2/s. These low values are again a result of three-dimensionality in the thermal-wave propagation problem, where the one-dimensional (1-D) expression, Eq. (56a), was used for the calculation of α_p, and were also measured in earlier work with three-dimensional PPE geometries.[18] The important conclusion from Fig. 5 is the exponential decay of the PPE voltage with $f^{1/2}$, in agreement with a Pd-surface work-function temperature modulation mechanism, as advanced by Balasubramanian *et al.*[17] for the Pd-mica-inert electrode system, and described by the model leading to Eq. (56a) above.

The ambient temperature dependence of the 100% H_2-saturated PPE signal was also monitored between -63 and $+50$ °C (Fig. 6). A slight decrease in the signal with increasing T was found, best described by the relationship

$$\Delta V_{\rm sat}(T)\simeq \text{const}\times T^{-1.4\pm0.15}. \tag{58}$$

The experimental results of Fig. 4 seem to support the domination of the PPE signal by the pyroelectric coefficient dependence on the concentration [H] in the Pd metal and specifically at the Pd-PVDF junction. The power dependence of the signal ($\sim f^{-0.7\pm0.2}$), as well as the measurability of the H_2 effect on the sensor at frequencies much higher than the thermally thick boundary value of 22 Hz, are indicative of bulk PVDF contribution to the signal, in agreement with our model leading to Eq. (53). The discrepancy between the observed and the ideal f^{-1} dependence must be sought in the fact that Eq. (53) is strictly valid for one-dimensional geometries, unlike the setup used in these experiments.

On the other hand, the behavior of Fig. 5 is consistent with the dominance of the PPE voltage by the Pd work-function dependence on the modulated thermal-wave temperature, a purely back-surface effect, with the "front surface" being the irradiated one. This mechanism appears to be similar to that described by Balasubramanian *et al.*[17] for the Pd-mica-Au sensor. In reconciling the two different dominances represented by the data in Figs. 4 and 5, it is reasonable to conclude that when a given interfacial (dipole) charge density $\sigma_f^{(\rm PPE)}(\omega)$ has been introduced at the Pd-PVDF junction, the bulk PVDF-induced polarization change dominates the signal generation, while the small thermal-wave-related synchronous temperature oscillations of the Pd layer are incapable of significantly altering $\sigma_f^{(\rm PPE)}(\omega)$. This tends to pin the value of p_z[H], and the frequency changes then would affect the average thermal-wave field in the pyroelectric. The result would be a power-law dependence with a rigid signal level shift with respect to the PPE signal without H_2 exposure, as observed in Fig. 4(b), and predicted by Eqs. (34) and (53). When the initial interfacial charge density is zero, however, as in the case of Fig. 5, the interaction of adsorbed and absorbed hydrogen with the Pd metal plays the predominant role; specifically, the Pd work-function dependence on the thermal-wave-related ac heating controls the PPE signal as it controls the [H] concentration available for interfacial accumulation in each frequency, in which case the pyroelectric property is irrelevant and the device operates in a simple purely photothermal mode.[17]

Further evidence for the domination of the mechanism described by the pyroelectric coefficient dependence on [H], with a preexisting interfacial density $N_{\rm H}$, Eq. (53), is offered from the consideration of the *sign* of the interfacial charge density on the PVDF side of Fig. 3. If a negative charge density, $-|\sigma_{\rm PPE}(\omega,t)|$, is substituted in the development of Eqs. (30)–(34), it yields

$$\langle P_n\rangle = \tfrac{1}{2}\sigma^+[\rm H] - |P_n^{(\rm PPE)}| \tag{59}$$

in lieu of Eq. (46), and

$$p_z[\rm H] = \left(\frac{\partial}{\partial T}\langle m_z\rangle - \alpha_v\langle m_z\rangle_T\right)N_{\rm H} - |p_z[0]| \tag{60}$$

instead of Eq. (50). Therefore, depending on the sign of the PVDF surface charge density, Eq. (53) predicts

$$|\Delta V_I^{\pm}(\omega,[H])| = \text{const} \times (\text{const} \times N_H \pm |p_z[0]|), \tag{61}$$

or, taking the absolute value of the voltage amplitude, as is done with the lock-in detection,[2]

$$|\Delta V_I^{\pm}(\omega,[H])| = \text{const} \times |\,|p_z[0]| \pm \text{const} \times N_H|. \tag{61'}$$

Figure 7 shows this exact behavior. Toward this goal, two PVDF films were coated with 285-Å Pd on oppositely polarized surfaces. It can be seen that the positively polarized electrode gives a normalized voltage, $|V_{A+}|/|V_R|$, which increases as a function of time, while the voltage from the negatively polarized electrode, $|V_{A-}|/|V_R|$, decreases in a manner essentially symmetric with respect to the equilibrium (i.e., $N_H = 0$) level. This behavior at a fixed modulation frequency strongly indicates the interfacial nature of the operating mechanism. If the contact potential shift were dominant, there should be no difference between the signals from oppositely polarized pyroelectrics, as long as the Pd-pyroelectric-inert metal geometry remains unaltered [Eqs. (25') and (55)].

Finally, the temperature dependence of the device behavior, measured over a broad low T (i.e., below room temperature) range for the first time with solid-state H_2 sensors, to the authors' best knowledge, offers a unique opportunity to use the Pd-PVDF junction for the study of the physics of hydrogen-Pd-polymer interaction. In the model of the change of the z-axis projection of the pyroelectric coefficient vector by the absorbed hydrogenic dipole field, as expressed by Eq. (50), the absorbed hydrogen atom may be viewed as a proton-displaced electron cloud dipole, as shown in Fig. 3. Each dipole pole close to the junction will induce an image charge in the dielectric (pyroelectric), so that an electrostatic potential will be created in the pyroelectric, corresponding to the presence of an "image dipole" in the field of the photothermally induced polarization $\mathbf{P}_{PPE}(\omega,t)$, and in agreement with Eq. (43).

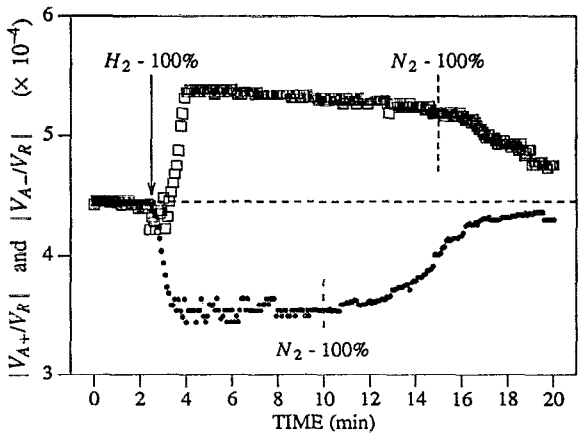

FIG. 7. (□) Variation of $|V_{A+}|/|V_R|$ as a function of time. (●) Variation of $|V_{A-}|/|V_R|$ as a function of time.

The hydrogenic image dipole moment vector may now be considered to perform two main motions in the thermodynamic environment of the pyroelectric matrix at temperature T: An axial oscillation, which varies its length at any instantaneous rotation angle θ about the polarization field z axis, and a libration about the z axis. These two motions can be assumed to be decoupled and each one has its own equilibration time constant. The main contribution to $\hat{n}\cdot\mathbf{p}(T)$ in Eq. (50) in the presence of the oscillating, librating image dipole moment vector is from the term $\partial\langle m_z\rangle_T/\partial T$; the second term is proportional to α_v and its contribution is known to be small compared to the first term in molecular dipole electrets.[19] Therefore, Eq. (50) becomes

$$\Delta p_z([H];T) \equiv p_z([H];T) - p_z([0];T) \simeq \left(\frac{\partial}{\partial T}\langle m_z\rangle_T\right) N_H. \tag{62}$$

Note that the temperature dependence of the pyroelectric coefficient of the unexposed PVDF can be effectively normalized out experimentally by taking the difference signals between the saturated level of the H_2 exposed device and the background PPE signal following exposure at any T. Under these conditions Δp_z only depends on the dipole density, N_H, and the thermostatistical factor $\partial\langle m_z\rangle_T/\partial T$. Due to the assumed independence of the vibrational and librational motions,

$$\frac{\partial}{\partial T}\langle m_z\rangle_T = \frac{\partial}{\partial T}\langle m_0 \cos\theta\rangle_T$$
$$= \langle\cos\theta\rangle_T \frac{\partial}{\partial T}\langle m_0\rangle_T + \langle m_0\rangle_T \frac{\partial}{\partial T}\langle\cos\theta\rangle_T. \tag{63}$$

For a thermal harmonically oscillating dipole, the rms amplitude of vibration is given by[19]

$$\langle m_0\rangle_T = \sqrt{\langle m_0^2\rangle_T} = \frac{1}{\omega_v}\left(\frac{2k_BT}{I}\right)^{1/2}, \tag{64}$$

where ω_v is the vibrational angular frequency, and I is the moment of inertia. Furthermore, the rms value of the projectional angle θ of libration with respect to the direction of the polarization field $\mathbf{P}_{PPE}(\omega,t)$ (the latter field assumed stationary with respect to the fast librating dipole, $\omega_l \gg \omega$) is[20]

$$\langle\cos\theta\rangle_T = -L\left(\frac{P_n^{(PPE)}}{\chi_e\epsilon_0 k_BT}\right) \simeq \frac{-P_n^{(PPE)}}{3\chi_e\epsilon_0 k_BT}, \tag{65}$$

where $L(a)$ is the Langevin function:

$$L(a) = \coth a - (1/a) \simeq a/3 \quad (a \ll 1). \tag{66}$$

The negative sign is necessary in Eq. (65) because the image dipole $\mathbf{m}$ in the PVDF is antiparallel to the polarization field $\mathbf{P}_{PPE}$ and changes the sign of the expression for the energy $-\mathbf{m}\cdot\mathbf{P}_{PPE}/\chi_e\epsilon_0$.

Equations (63)–(65) give

$$\frac{\partial}{\partial T}\langle m_z\rangle_T = \frac{\sqrt{2}}{6}\left(\frac{P_n^{(\mathrm{PPE})}}{\chi_e \epsilon_0 \omega_\nu \sqrt{k_B I}}\right)\frac{1}{T^{3/2}}, \tag{67}$$

which yields a $T^{-1.5}$ dependence for the pyroelectric coefficient change $\Delta p_z([\mathrm{H}];T)$ in Eq. (62), in agreement with Fig. 6. Physically, the decrease in the saturation PPE signal in the presence of H_2 with temperature can be understood as due to a thermostatistical decrease of the mean librating hydrogenic dipole moment with a temperature-induced increase in the rms fluctuation angle $\langle\theta\rangle$ and the concomitant increased libration amplitude, as discussed by Broadhurst and Davis.[7] It is interesting to mention that a Pd work-function thermal-wave temperature modulation mechanism as proposed by Balasubramanian *et al.*[17] leads to a T^{-2} theoretical signal dependence.

IV. CONCLUSIONS

A Pd-PVDF junction model was developed based on the photothermal response of the pyroelectric. It was shown that detailed electrostatic theory is consistent with either, or both, of two operating mechanisms for H_2 gas detection: One involving the pyroelectric coefficient dependence on the absorbed H-dipole density at the junction, and the other involving the contact potential shift in the presence of hydrogen as a result of the thermal-wave modulation of the [H]-dependent Pd work function.

Experimental results with the sensor were supportive of both mechanisms, depending on experimental conditions. The theory is able to account for the behavior of nonpyroelectric photothermal sensors of the type fabricated by Balasubramanian *et al.*[17] and gives good agreement with low-T measurements upon invocation of a statistical mechanism based on hydrogenic image dipoles performing independent vibrational and librational motions about the polarization field (z) axis.

ACKNOWLEDGMENT

The support of the Ministry of Energy, Mines, and Resources Canada through a contract to the Center for Hydrogen and Electrochemical Studies (CHES) is gratefully acknowledged.

[1] H. Coufal and A. Mandelis, Ferroelectrics **118**, 379 (1991).
[2] A. Mandelis and C. Christofides, Sensors and Actuators B **2**, 79 (1990).
[3] C. Christofides and A. Mandelis, J. Appl. Phys. **66**, 3975 (1989).
[4] A. Mandelis and C. Christofides, J. Vac. Sci. Technol. A **8**, 3980 (1990).
[5] J. N. Zemel, in *Solid State Chemical Sensors*, edited by J. Janata and R. J. Huber (Academic, New York, 1985), Chap. 4.
[6] R. K. Wangsness, *Electromagnetic Fields* (Wiley, New York, 1986), Chap. 10.
[7] M. G. Broadhurst and G. T. Davis, in *Electrets*, Vol. 33 of *Topics in Applied Physics*, 2nd ed., edited by G. M. Sessler (Springer, Heidelberg, 1987), Chap. 5.
[8] A. Mandelis and M. M. Zver, J. Appl. Phys. **57**, 4421 (1985).
[9] I. Lundström, Sensors and Actuators **1**, 403 (1981).
[10] I. Lundström, M. S. Shivaraman, and C. Svensson, J. Appl. Phys. **46**, 3876 (1975).
[11] I. Lundström, M. S. Shivaraman, C. Svensson, and L. Lundkvist, Appl. Phys. Lett. **26**, 55 (1975).
[12] I. Lundström, M. S. Shivaraman, and C. Svensson, Surf. Sci. **64**, 497 (1977).
[13] H. B. Michaelson, IBM J. Res. Dev. **22**, 72 (1978).
[14] J. Horiuti and T. Toya, in *Solid State Surface Science*, Vol. 1, edited by M. Green (Dekker, New York, 1969), pp. 1–86.
[15] I. Lundström and C. Svensson, in *Solid State Chemical Sensors*, edited by J. Janata and R. J. Huber (Academic, New York, 1985), Chap. 1.
[16] M. C. Nelson, D. M. Hanson, and J. S. Patel, Chem. Phys. **116**, 311 (1987).
[17] A. Balasubramanian, J. J. Santiago-Aviles and J. N. Zemel, J. Appl. Phys. **69**, 1102 (1991).
[18] M. Mieszkowski, K. F. Leung, and A. Mandelis, Rev. Sci. Instrum. **60**, 306 (1989).
[19] F. I. Mopsik and M. Broadhurst, J. Appl. Phys. **46**, 4204 (1975).
[20] A. J. Dekker, *Solid State Physics* (Prentice-Hall, Englewood Cliffs, NJ, 1956), Sect. 6-3.